# Chapter 3

# The Antiproton Trap

Antiprotons are created, collected, and decelerated at CERN. The lowest energies available for experimentation are still around 5.9 MeV. A major challenge of the mass comparison experiment in a Penning trap is to load antiprotons, only available from an external high energy source. This places new constraints on the trapping apparatus not previously required for earlier studies using electrons, protons, and other common ions. In this chapter, we cover some of the major apparatus requirements, design criteria, and solutions so that the trap can be interfaced to the CERN accelerator complex which serves as an antiproton source.

## 3.1 Open Endcap Trap

Previous high precison measurements of charged particles such as electrons and protons, have been done in traps with electrodes shaped along equipotentials of the desired quadrupole potential. Protons and electrons are typically loaded by passing an electron beam through the trap where neutral atoms in the trap region are ionized, and then confined in the properly biased harmonic potential well. Since antiprotons must be obtained from an external high energy source, with a FWHM beam diameter often on the order of 1 cm, it is necessary to provide larger access to the trap than the small holes and slits often used in hyperbolic traps. In addition, the antiproton capture efficiency (Chapter 4) is proportional to the length of the trapping region making a very long trap advantageous.

For the purpose of access and particle confinement, cylindrical Penning traps

with long, open endcap electrodes have been previously used. In 1965 such a device was used to produce polarized electron beams [15]. Long cylindrical traps have also been used for the containment and study of cold electron plasmas [70]. In 1986, for an earlier version of our present work, we used a simple three electrode cylindrical trap to capture antiprotons in an ion trap for the first time [37]. Recently, cylindrical style traps have also been used for experiments requiring access for lasers [51] and cold neutron beams [16].

A much purer electric quadrupole potential is required for precise studies of elementary particles when the trap is an important part of the bound system. For purposes of access to an antiproton source and the requirements for mass spectroscopy, we have developed an open endcap consisting of a series of cylindrical electrodes shown in Fig. 3.1. This trap is unique in that it allows for adjusting the purity of the quadrupole potential without affecting the depth of the harmonic well [43].

### 3.1.1 A Tunable Quadrupole From Cylindrical Electrodes

By careful selection of the trap electrode dimensions and with appropriate biasing, we have designed and constructed an orthogonalized, tunable cylindrical trap. The cylindrical trap scheme can thereby produce an extremely good quadrupole potential over a small region in the trap center where the contained particles reside 3.2.

The electric potential at the center of the trap can be described by an expansion of Legendre polynomials

$$V = \frac{1}{2} V_0 \sum_{k=0}^{\infty} C_k \left(\frac{r}{d}\right)^k P_k(cos\theta) \tag{3.1}$$

where $V_0$ is the potential difference applied between the ring and endcap electrodes of the ideal three electrode trap. The variable $d$ is the characteristic size of the trap defined in Eq. 2.5, $P_k(\cos\theta)$ is the $k^{th}$ Legendre polynomial, and $C_k$ is a dimensionless weighting coefficient.

For a perfect electric quadrupole, all coefficients other than $C_0$ and $C_2$ in the expansion 3.1 are zero. For the cylindrical trap, $C_2$ is less than unity reflecting

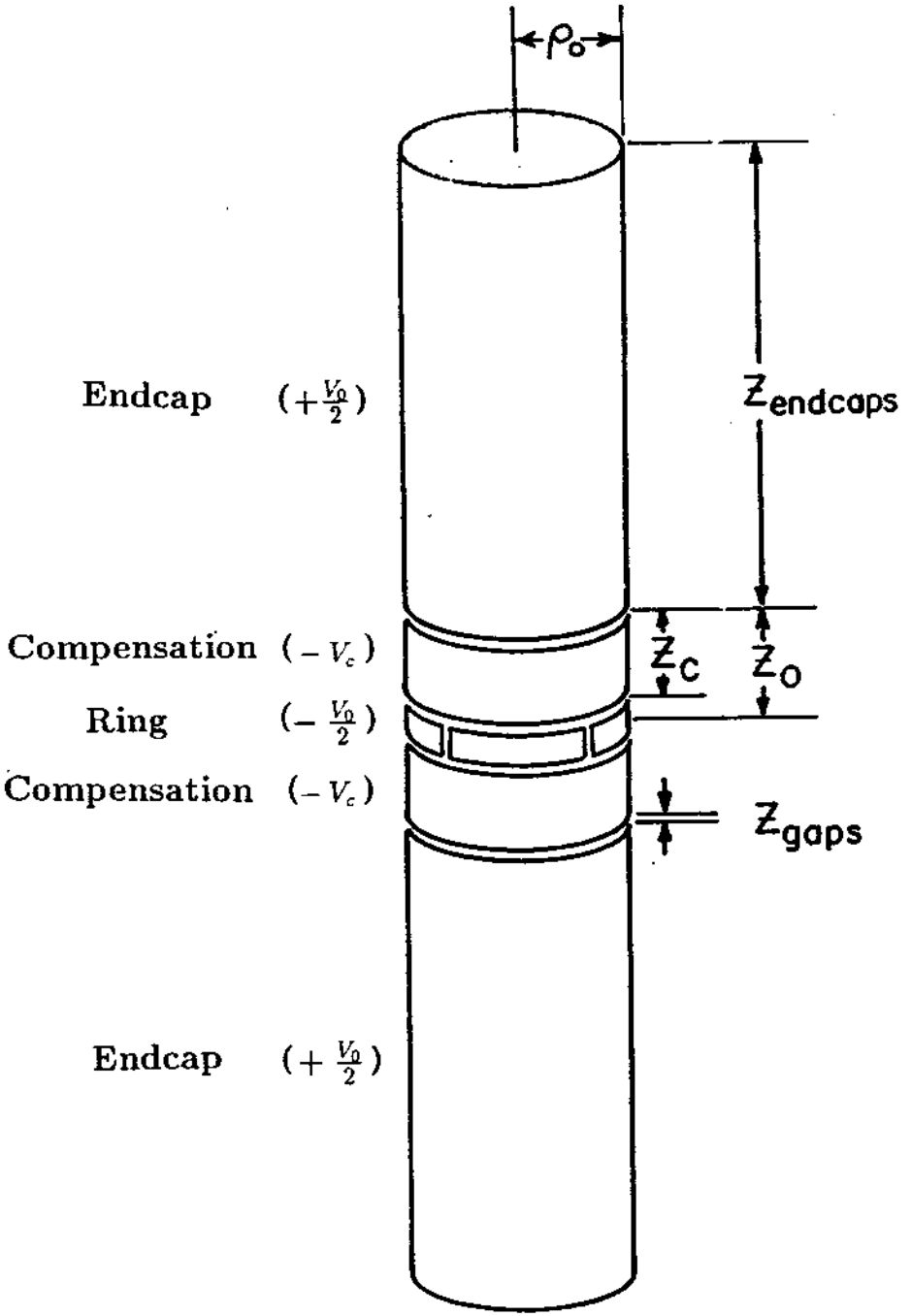


Figure 3.1: The open-endcap compensated cylindrical Penning trap.

a deviation from the hyperbolic electrode geometry (with $C_2 = 1$ resulting from electrodes along the hyperbolic surface $r^2 P_2(\cos\theta)$=constant). In the more general case the axial oscillation frequency of a particle of mass m, and electric charge q, resulting from the quadrupole field weighted by $C_2$ is

$$\omega_z^2 = \frac{qV_0}{md^2} C_2. \tag{3.2}$$

Cylindrical 'compensation' electrodes shown in Fig. 3.1 provide for tunability. Since the trap has reflection symmetry about the plane z=0, higher order terms that contribute to anharmonicity are the next even order terms $C_4$ and $C_6$. These terms can be compensated by adjusting the potential $V_c$ applied to the two compensation electrodes.

It is most convenient to analyze the potential near the trap center (defined as the origin) as the superposition of two separate boundary value problems [30]. The superimposed potential resulting from the two boundary conditions is

$$V = V_0\phi_0 + V_c\phi_c = \frac{1}{2}V_0 \sum_{k=0}^{\infty} C_k \left(\frac{r}{d}\right)^k P_k(cos\theta) \tag{3.3}$$

where

$$\phi_0 \equiv \frac{1}{2}\sum_{k=0}^{\infty} C_k^{(0)} \left(\frac{r}{d}\right)^k P_k(cos\theta), \tag{3.4}$$

and

$$\phi_c \equiv \frac{1}{2}\sum_{k=0}^{\infty} D_k^{(0)} \left(\frac{r}{d}\right)^k P_k(cos\theta). \tag{3.5}$$

The potential $\phi_0$ is due to a potential of -1/2 applied to the ring and +1/2 applied to the endcaps, with the compensation electrodes grounded. The potential $\phi_c$ is due to a potential of 1 applied to the compensation electrodes with all other electrodes grounded. The coefficients $C_k^{(0)}$ and $D_k^{(0)}$ are solved in the standard way by equating the above expansions to the applied potential along the appropriate boundary and integrating over the orthonormal set of Legendre polynomials and the small term $(r/d)^k$.

From 3.3, the expansion coefficients $C_k$ can be expressed in terms of the others by

$$C_k = C_k^{(0)} + D_k \frac{V_c}{V_0}. \tag{3.6}$$

Adjusting $V_c$ thus offers the possibility to make $C_4$ to improve the trap harmonicity. From Eq. 3.6 the optimum tuning ratio is

$$\left(\frac{V_c}{V_0}\right)_{C_4=0} = \frac{-C_4^{(0)}}{D_4}. \tag{3.7}$$

This is it is highly desirable that the leading order anharmonic coefficient $C_4$=0, since this along with higher order coefficients is responsible for amplitude (energy) dependent shifts of the particle axial frequency. The shift is approximately

$$\frac{\Delta\omega_z}{\omega_z} = \frac{3}{2}\frac{\widetilde{C_4}}{C_2}\frac{E_z}{qV_0C_2} \tag{3.8}$$

where $E_z$ is the energy in the axial motion and

$$\widetilde{C_4} = C_4 + \frac{5}{2}C_6\frac{E_z}{qV_0C_2} \tag{3.9}$$

takes into account $C_4$ and the next higher order term $C_6$ [30].

Another useful potential scheme applied to the trap is an antisymmetric potential $\pm V_A/2$ to either the endcaps or the compensation electrodes [31]. Under such boundary conditions, expansion 3.1 will only consist of odd terms. The leading order odd term k=1 has the effect of applying a linear electric field across the center. This has applications for deliberately displacing the confined particles, and is relevant for particle detection (discussed in Chapter 5). The potential within the trap is given by

$$V = V_A\phi_A. \tag{3.10}$$

The solutions to Laplace's equation $\phi_A$ which satisfies the antisymmetric boundary condition $\pm V_A/2$ to the endcap or compensation electrodes respectively are

$$\phi(\mathbf{r})_{A,c} = \frac{1}{2}\sum_{k_{odd}=1}^{\infty} c_k\left(\frac{r}{z_0}\right)^k P_k(cos\theta) \tag{3.11}$$

and

$$\phi(\mathbf{r})_{A,d} = \frac{1}{2}\sum_{k_{odd}=1}^{\infty} d_k\left(\frac{r}{z_0}\right)^k P_k(cos\theta). \tag{3.12}$$

The size of the lowest order coefficients $c_1$ and $d_1$ are very useful for issues regarding particle detection and damping.

The computation for our open endcap trap was carried out by Gabrielse, Haarsma, and Rolston [43] following an earlier analysis by Gabrielse and MacKintosh on a related cylindrical geometry but with flat endcaps[32].

The relative dimensions $\rho_0/z_0$ and $z_c/z_0$ are chosen such that $D_2$=0 so that the trap is orthogonalized. Equation 3.6 implies that $C_2 = C_2^{(0)}$. Detailed figures, showing critical trap coefficients as a function to the relative trap dimensions $\rho_0/z_0$ and $z_c/z_0$ are found in reference [43].

The relative dimensions chosen for the antiproton trap, and the calculated coefficients corresponding to the multipole expansion about the trap center are shown in Table 3.1. We note $D_4$ is sufficiently large so that $C_4$ can be tuned using reasonable potentials. For a given trap, it is desirable to minimize the quality factor $\gamma \equiv D_2/D_4$ [13]. From 3.6, $C_4$ is calculated to be minimized with a potential applied to the compensation electrodes of $V_c = -0.381V_0$ where $V_0/2$ is applied to the endcap, and $V_0/2$ is applied to the ring (for $V_0$ applied to the ring with the endcaps held at ground, the compensation potential is expressed by $V_c = 0.8809V_0$). . In addition, the selected relative dimensions also have the feature that at the optimal tuning point $V_c/V_0$ to make $C_4$=0, then $C_6 = C_6^{(0)} + (0.3811)D_6 = 0$. From 3.8 and 3.9, the advantages of this scheme are evident.

The potential in the cylindrical trap resulting from the chosen relative dimensions is shown in Fig. 3.2. The quadrupole field resulting from a hyperbolic shaped trap with the same effective dimension $\tilde{d} = d/\sqrt{C_2}$ is superimposed in the dashed lines to illustrate the effectiveness of this scheme for producing a quadrupole region in the trap center.

There are several competing criteria for choosing the absolute trap size. First, access is needed to obtain a good antiproton trapping efficiency requiring a reasonable size for $\rho_0$ and as long as trap as practical. The antiproton beam when optimally focussed can have a FWHM diameter of 2 mm, though the beam diameter can often be on the order of 1 cm. Second, the effectiveness of particle resistive detection and damping (Chapter 5) depends on the trap dimensions. For the axial motion, the detected signal is proportional to $(d_1/z_0)^2$ if the detection is on the compensation electrode, and $(c_1/z_0)^2$ if the detection is on the endcap

Table 3.1: (a) The relative trap electrode size to produce an compensated cylindrical Penning trap. (b) Expansion coefficients calculated for several useful boundary conditions. (c) Measured trap coefficients.

### (a) Relative Electrode Sizes to Produce $D_2 = 0$ and $C_6 = 0$

| | | |
|---|---|---|
| Radius | $\rho_0/z_0$ | $= 1.0239$ |
| Compensation Electrodes | $z_c/z_0$ | $= 0.8351$ |
| Endcap Electrodes | $z_{endcaps}/z_0$ | $= 4.312$ |
| Gaps Between Electrodes | $z_{gaps}/z_0$ | $= 0.0303$ |
| Tuning Ratio for Minimal $C_4$ | $V_c/V_0$ | $= 0.3811$ |

### (b) Expansion Coefficients

$C_2^{(0)} = 0.5449$
$C_4^{(0)} = -0.2119$
$C_6^{(0)} = 0.1638$
$C_8^{(0)} = -0.1359$

$D_2 = 0$
$D_4 = -0.5560$
$D_6 = 0.4300$
$D_8 = 0.2609$

$C_2 = 0.5449$
$C_4 = 0$
$C_6 = 0$
$C_8 = -0.0365$
$C_0 = 0.775$

$c_1 = 0.3346$
$c_3 = 0.2202$
$c_5 = -0.0385$

$d_1 = 0.8994$
$d_3 = -0.8439$
$d_5 = 0.3915$

### (c) Measured Coefficients

$C_2 = 0.551$
$D_2 \leq 0.005$
$C_4 << 0.0008$

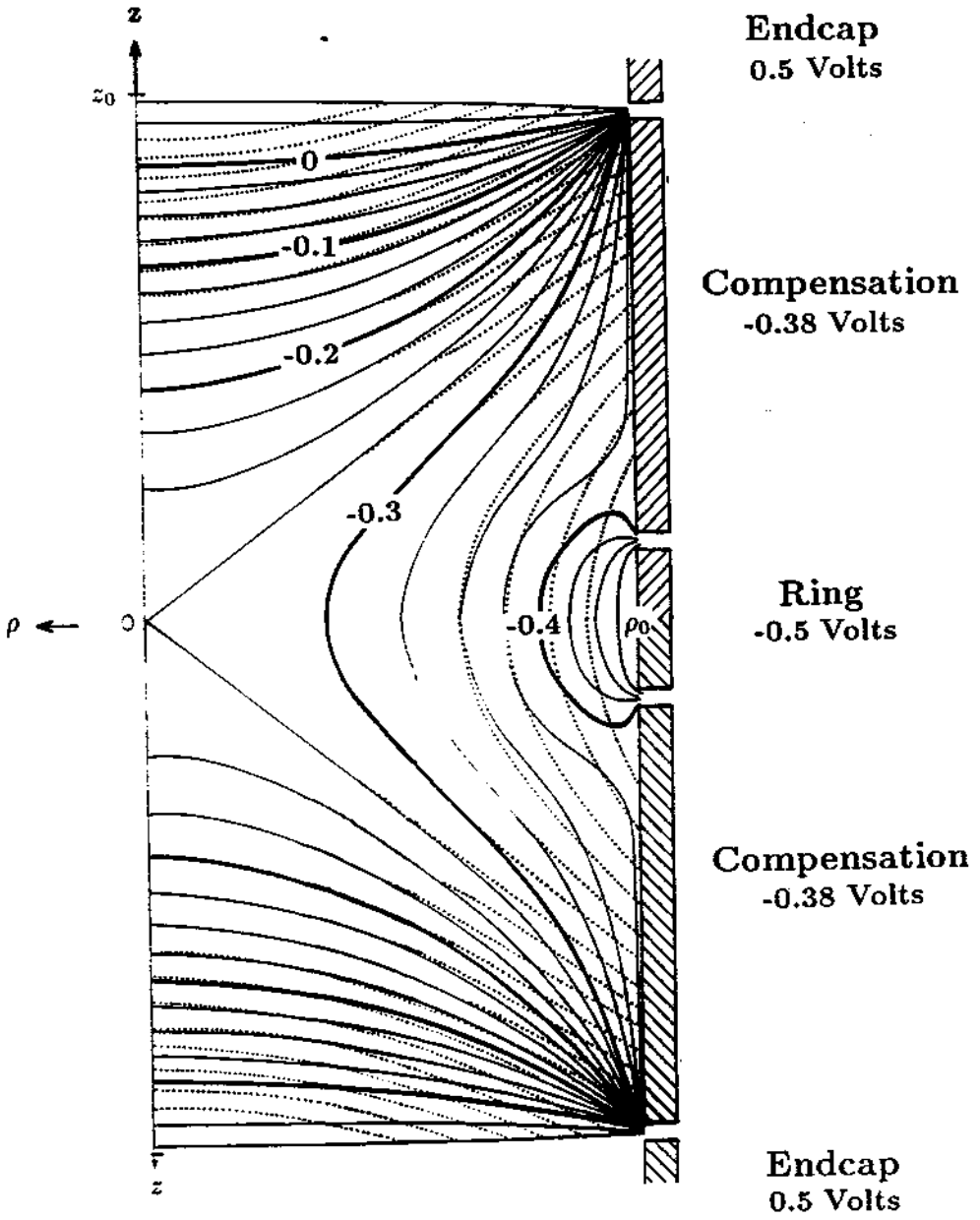


Figure 3.2: Electrostatic equipotential field lines in the compensated, open-endcap trap (solid) compared with the field lines for an ideal quadrupole potential (dotted).

electrode. For detection and damping a small $z_0$ (and $\rho_0$) is desirable. Finally, perturbations of the uniform magnetic field and the ideal quadrupole potential in the center of the trap where the confined particles reside become smaller the farther away the trap electrodes are. In addition, measurements in a larger trap will be much less sensitive to trap asymmetries and misalignment as shown in 2.22 a large trap makes the frequency hierarchy in Eq. 2.15 more pronounced.

With emphasis on loading and cooling antiprotons, we constructed a trap with the dimensions and resonant frequencies given in Table 3.2 and shown in Fig. 3.1. (If needed, we could later transfer the cooled antiprotons to a traditional hyperbolic trap with a small access hole). This trap has a characteristic dimension of $d/\sqrt{C_2}$=0.693 cm which for typical fields and trapping potentials results in $(\overline{\nu}_z\ /\overline{\nu}_c')^4 \approx 2\times 10^{-7}$ for antiprotons. The tradeoffs in the selected trap size will become more apparent when we discuss particle detection and damping (Chapter 5), and systematic perturbations due to the location and condition of the trap electrodes (Chapter 10).

### 3.1.2 Construction Issues

In practice our trap is slightly more complicated than the five electrodes discussed above. To allow direct detection and damping of $\nu_c'$ the ring electrode is divided into quadrants [97]. To allow sideband cooling of the magnetron motion [114], the compensation electrodes are each split into 2 segments. These vertical slits have not been taken into account in the coefficient calculations [43].

To minimize distortion of the magnetic field, the trap electrodes are constructed of OFHC copper. The electrodes are spaced, interlocked, and self aligned using small MACOR rings, all of these pieces are machined to tolerances of 0.005 mm (0.0002") [1]. The gaps between the electrodes are 0.18 mm and the depth to width of the gap is 9.2 so that any exposed MACOR or sapphire is sufficiently screened electrostatically. The ring and compensation electrodes were sectioned with electric discharge machining (EDM) and have sectioned gap widths of 0.15

[1]Throughout the remainder of this chapter, dimensions are ocassionally reported in inches (1"=2.54 cm) if it better describes a standard material size or machining dimension.

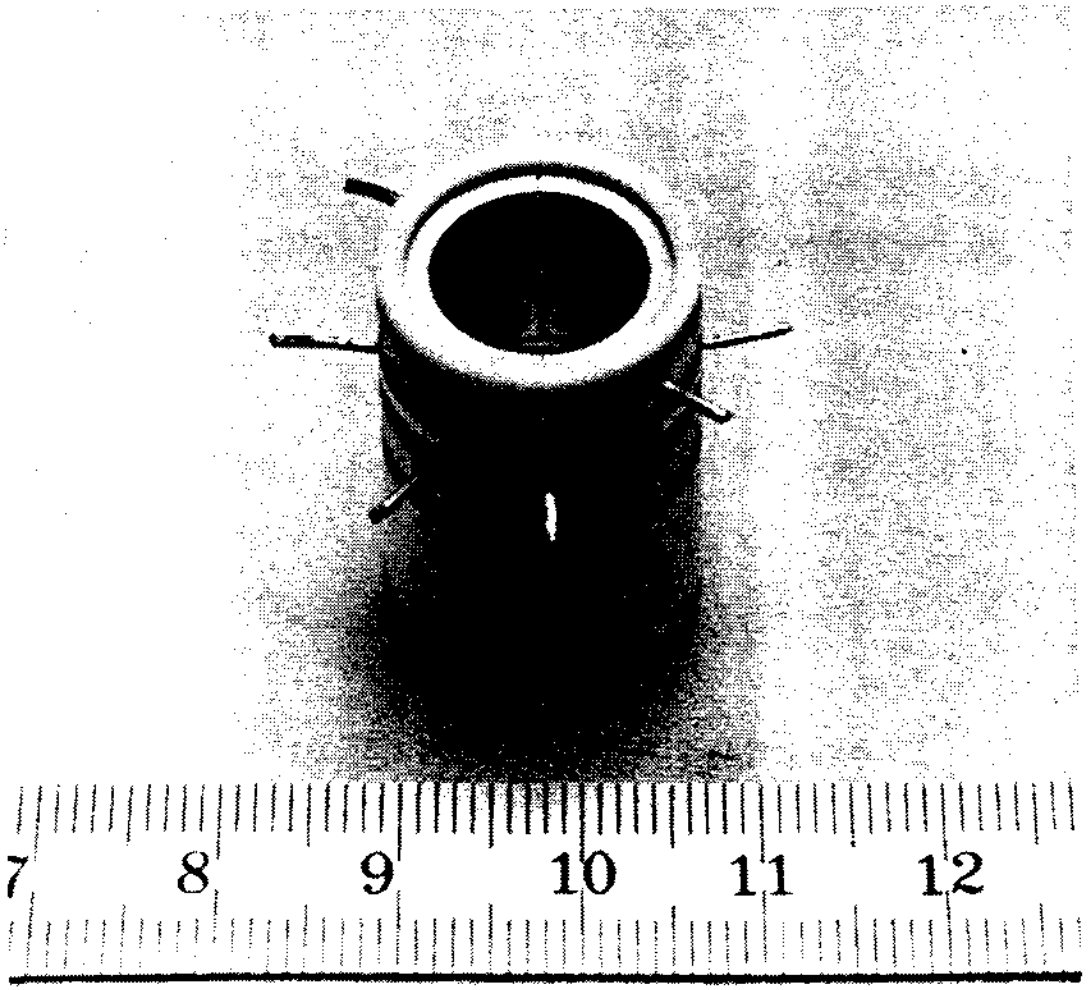


| | |
|---|---|
| Radius | $\rho_0 = 0.6000$ cm. |
| Length | $z_0 = 0.5860$ cm. |
| Characteristic Dimension | $d = 0.5116$ cm. |
| Effective Dimension | $d/\sqrt{C_2} = 0.6931$ cm. |

Figure 3.3: The open endcap trap showing the assembled split compensation and quad ring electrodes (scale in cm).

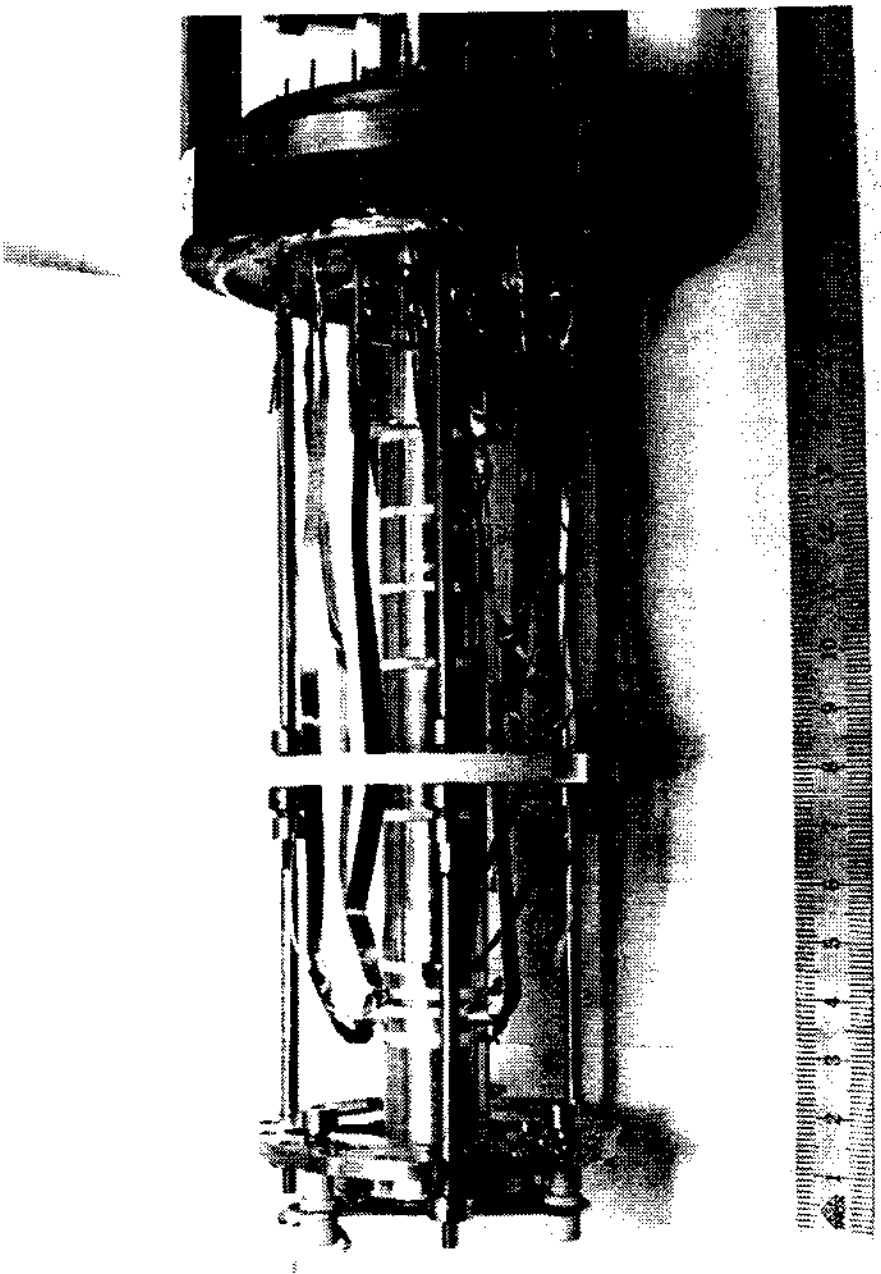

Figure 3.4: The extended cylindrical trap mounted from the upper flange of the trap vacuum enclosure (scale in cm).

Table 3.2: Typical eigenfrequencies for chosen trap dimensions and field strengths.

| **Electrons:** | **Antiprotons (Protons):** |
|---|---|
| $\nu_z(e^-)$=9.63152 $V_0^{1/2}$ MHz/$\sqrt{Volt}$ | $\nu_z(\overline{p})$ =0.22477 $V_0^{1/2}$ MHz/$\sqrt{Volt}$ |
| $\nu_c\ (e^-)$=27.99225 $B_0$ GHz/Tesla | $\nu_c\ (\overline{p})$ =15.24507 $B_0$ MHz/Tesla |
| $V_0$=+32 V, $B_0$ ≈5.86 T | $V_0 = \pm 71$ V, $B_0$ ≈5.86 T |
| $\nu_z\ (e^-) = 54$ MHz | $\nu_z\ (\overline{p}) = 1.9$ MHz |
| $\nu_c\ (e^-) = 164$ GHz | $\nu_c\ (\overline{p}) = 89.3$ MHz |
| $\nu_m\ (e^-) = 9.1$ kHz | $\nu_m\ (\overline{p}) = 20$ kHz |

mm. The segments are azimuthally separated and aligned with 1 ± 0.005 mm diameter sapphire spheres. The copper electrodes have been plated with a 0.2 $\mu$m diffusion barrier of rhodium and a 2 $\mu$m layer of gold to avoid oxidation and minimize possible surface charge accumulation. surface charge. The harmonic region of the constructed trap is shown in Fig. 3.3 and Fig. 3.5 shows the location of the sapphire spheres.

For purposes of containing high energy antiprotons, the trap is lengthened by additional cylindrical segments as shown in Fig. 3.4 to increase the trapping efficiency during the loading process (Chapter 4). This long trap is sufficient for confining high energy antiprotons, though it is not a harmonic trap in this configuration.

This long electrode configuration consisting of several segments may be useful as a storage trap. Another possible use could be in a 'nested trap' mode [38] where opposite charge species can be simultaneously confined. This scheme can be used to study charge exchange and recombination mechanisms, and may be a possible environment for the formation of antihydrogen by merging antiprotons with confined positrons [38,40,41].

### 3.1.3 Calculated Magnetic Bottle

Magnetic gradients can result from a distortion of the field by the magnetic susceptibility of the nearby material forming the trap electrodes and insulating spacers. The leading order effect of field distortions arising from the trap (which is symmetric about the plane z=0) is typically of the form of a magnetic bottle field. Intentional magnetic bottles in Penning traps have played a key role in measurements of electrons and positrons [86] since cyclotron and spin frequencies are only observable by coupling into the axial motion. For precision mass spectroscopy it is important to quantify and, in most cases, minimize the bottle field.

To keep such distortions small, our trap is constructed of OFHC copper which is only slightly diamagnetic. The insulating spacers consist of MACOR rings, and 1 mm diameter sapphire ($Al_2O_3$) spheres. The magnetization dipole moment per unit volume of the trap in a 5.9 T field at 4 K for the relevant materials are (in cgs units)

| | | |
|---|---|---|
| M(Cu) | = –0.05 | ref. [64] |
| M(MACOR) | = +0.78 | ref. [93] |
| M(MACOR) | = +0.52 | ref. [58] |
| M($Al_2O_3$) | = -0.085 | ref. [64] |

The magnetization of sapphire and copper are small and they are diamagnetic. The MACOR is the dominant contribution.

We calculate the field distortion following Brown and Gabrielse [13]. The magnetic field perturbation near the trap center resulting from a ring of material, with cross section $d\rho' dz'$, and located at the cylindrical coordinates $\rho'$,$z'$ (or $r'$,$\theta'$ in spherical coordinates) is given by

$$\Delta \mathbf{B}(\mathbf{r}) = \sum_{l=0}^{\infty} \beta_l r^l [P_l(\cos\theta)\hat{\mathbf{z}} - (l+1)^{-1} \sin\theta \frac{dP_l(\cos\theta)}{d\cos\theta}\hat{\rho}] \qquad (3.13)$$

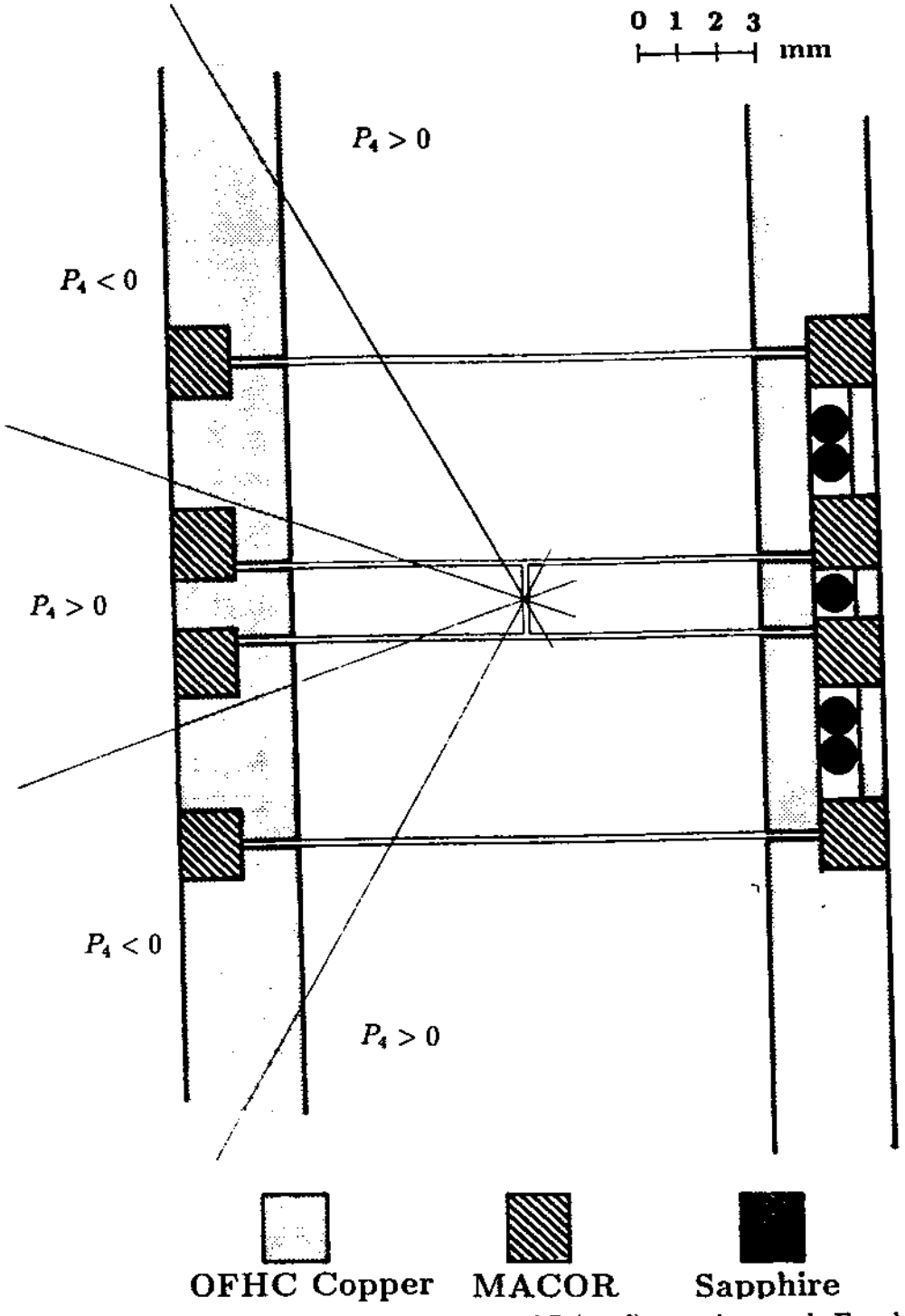


Figure 3.5: Open-endcap trap with the zeros of $P_4(cos\theta)$ superimposed. For clarity, the compensation electrodes are rotated azimuthally 45° and the endcap electrodes are truncated.

where

$$\beta_l = (l+1)(l+2)2\pi \int \rho' d\rho' dz' M(\rho', z')(r')^{-l-3} P_{l+2}(\cos\theta') \qquad (3.14)$$

The leading term $\Delta \mathbf{B_0} = \beta_0 \hat{\mathbf{z}}$ adds to the homogenous magnetic field. When the trap is symmetric under reflection z → -z, the integral in Eq. 3.13 vanishes for odd $l$ so that $\beta_1 = 0$. The $l = 2$ term (often called a magnetic bottle), is

$$\Delta \mathbf{B_2}(\mathbf{r}) = \beta_2 r^2 [\frac{1}{2}(3\cos^2\theta - 1)\hat{\mathbf{z}} - \sin\theta\cos\theta\hat{\rho}]. \qquad (3.15)$$

From 3.14, it is evident that material placed at the zeros of $P_4(\cos\theta')$ will produce no magnetic bottle (i.e. at $\theta' \approx 30°$ and $\theta' \approx 71°$). Since the sign of $P_4(cos\theta')$ changes at the zeros, the effect of material in one region in producing $\beta_2$ can be cancelled by an appropriate amount of material in a region where $P_4(\cos\theta')$ is of opposite sign. Figure 3.5 shows the open endcap trap with the zeros of $P_4(cos\theta')$ superimposed on it. It is evident from the figure that the bottle resulting from the two inner macor rings is partially compensated by the outer two rings. For our existing trap construction, the coeficients resulting from the four innermost MACOR rings (assuming M=+0.78) calculated using 3.14 are

$$\beta_0 = -0.53\ Gauss, \qquad (3.16)$$

and

$$\beta_2 \leq +0.84\ \frac{Gauss}{cm^2}. \qquad (3.17)$$

Referring again to Fig. 3.5 it is evident that the trap could be improved and $\beta_2$ could be made to vanish by adding the appropriate amount of MACOR to the two outer rings.

The change in the axial component resulting from the presence of the trap in the strong 5.9 T homogenous magnetic field causes a proportional shift in the particle cyclotron frequency. The effect of the bottle on the cyclotron frequency resulting from $\beta_2 = +0.84$ G/cm$^2$ is

$$\frac{\Delta B_z}{B} \leq 1.4 \times 10^{-5}(z^2 - \frac{\rho^2}{2}). \qquad (3.18)$$

where z and $\rho$ are measured in centimeters.

## 3.2 Trap Support and Cryogenic System

In many previous experiments where Penning traps have been used for high precision studies, the trap enclosure has been cryopumped and the detection electronics cooled to 4.2 K by immersing the apparatus in a bath of liquid helium. The need to interface the trap to an accelerator facility, led us to construct a cryogenic system where the the trap enclosure and the cooled pre-amplifiers reside in a vacuum and are heat sunk to a helium Dewar. This scheme has the major advantage that antiproton access into the magnet bore and to the trap is not impeded by liquid helium and the relatively thick wall enclosure necessary to make a liquid helium container.

The basic design consideration is to provide a liquid helium cooled support (or cold finger) to an enclosure containing the trap described in Section 3.1. This system must fit into a 100 mm diameter magnet bore (Section 3.3) and be able to hold the trap near 4.2 Kelvin in order to achieve the ultra-high vacuum necessary for sufficient antiproton containment times. It is also essential that the preamplifiers used for detecting the confined particle motions are as cold as possible in order to maximize signal to noise. Because of the frequency regime in which we operate (1-100 Mhz), it is necessary that this region be as close to the trap as possible to avoid capacitive coupling of the weak signals to ground before being detected. Other design constraints include the desire for long helium hold time, and the need to be able to remove, work on, and cycle the apparatus quickly.

### 3.2.1 Description

The developed trap support and cryogenic system consists of six modular components shown in Fig. 3.6. The whole system is assembled, wired, tested, and then lowered into the 100 mm diameter bore of a superconducting magnet. The following briefly describes each section of the apparatus required to hold and cool the open endcap cylindrical trap.

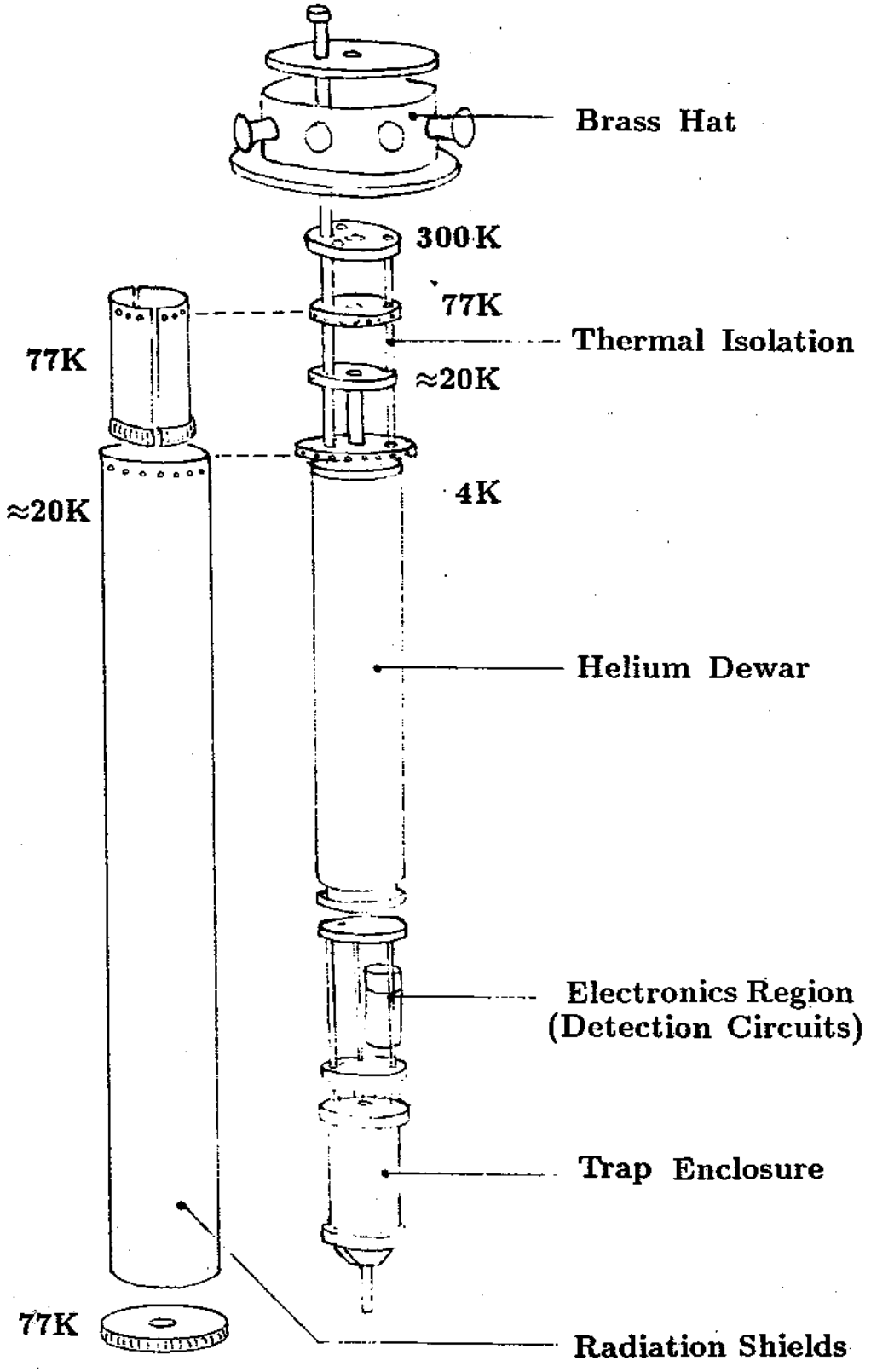


Figure 3.6: The cryogenic system shown assembled from its modular components.

### The Brass Hat

The trap apparatus is suspended from a brass structure (often referred to as the 'hat') which forms the upper vacuum enclosure of the vertical magnet bore. This hat contains all electrical, vacuum, and cryogenic access to the helium Dewar and the trap itself. All dc lines are passed through commercial 8-pin constantan vacuum feedthroughs [17] which are welded or hard soldered into standard quick flange blankoffs (Tube OD=1.5"). Over each multipin connector an aluminum box is mounted containing connections to standard 50 Ω bulkhead BNC connectors. RC or LC filters with various time constants prevent unwanted RF leakage onto the dc lines. There is also a liquid helium level sensor and a temperature sensor both of which have a calibrated resistance measured using a standard 4-wire technique. Six RF drive lines and three RF detection lines pass through 50 Ω SMA feedthroughs. Two standard SHV feedthroughs are used to apply high voltages.

### Thermal Isolation

A thermal isolation structure is constructed out of 0.375" ID G-10 tubing and 0.25" thick G-10 sheets[78]. G-10 is a strong, epoxied fiber-glass material with very low thermal conductivity. This structure contains a 0.005" thick, 0.5" OD stainless steel tube and bellows system that serve as the liquid helium fill and recovery access to the helium de mounted below. The fill tube is connected to the hat segment above and the helium Dewar below by stainless steel mini-conflat flanges. In addition this region has two OFHC copper plates which are heat sunk to the helium fill and recovery line. A shield constructed from a copper tube is bolted to the upper heat sinking plate and touches the bore of the magnet with silver plated copper beryllium 'fingers' [107] (the magnet bore can be independently kept at 77K). The lower heat sinking plate provides a mounting platform from which a floating thermal radiation shield is mounted. This shield fits over the entire apparatus and reduces the radiation load from the magnet bore to the trap enclosure at 4 K by shunting a portion of the radiative heat load to the helium gas in the recovery line. Finally the G-10 thermal isolation structure serves as a

guide for over 40 wires going to the trap.

The G-10 structure is assembled using small aluminum pins and epoxied together using Ren-Weld epoxy. Accurate assembly of this structure is critical to insure proper alignment and maximum performance of the cryogenic system. To keep tolerances tight, we epoxied this structure while it was jigged in a lathe.

### The Helium Dewar

The helium de itself is constructed of OFHC copper to prevent thermal gradients along its length as the helium level changes. We wish to avoid such gradients because they might result in very small helium level dependent shifts of the trap center with respect to the magnetic field. The Dewar also has two 0.25" ID tubes through it which serve as access for the dc and RF lines which go to the trap. In addition, a 0.5" ID copper tube passes through the center of the Dewar for possible future access to the center of the trap. The 0.5" access has been preserved in the hat, the thermal isolation stage and the electronics region. Two access ports into the top of the dewar are sealed using S.S. mini-conflat flanges. One port is connected to the helium fill and recovery tube, and the other with a four pin cryogenic feedthrough [17]. This feedthrough is attached to a 20" liquid helium level sensor consisting of a superconducting wire [1]. The wire resistance, monitored using a standard 4 wire technique, is proportional to the liquid helium level. The entire Dewar system was assembled using Cu-Ag eutectic solder in a controlled hydrogen atmosphere at $805°C$ . The top and bottom endplates were then faced off to ensure they were parallel. The bottom plate was subsequently gold plated for better heat sinking of the trap apparatus below.

### The Cold Electronics Region

This region consists of three OFHC 0.375" per side square copper rods connecting two OFHC copper plates which provide a support and heat sinking point for the tuned resonant circuits and FET amplifiers used for particle eigenfrequency detection (described in Chapter 5). These rods also serve as the 'cold finger' between the liquid helium Dewar above and the trap enclosure below. They are also

silver soldered but with lower temperature silver solder. This entire system is gold plated and is bolted to the Dewar above and the trap enclosure below with 48 M-4 brass screws to provide, by compression, good thermal conductivity across the joints [52]. Temperatures during cooldown are monitored with a calibrated carbon glass resistor[63] attached to this region.

### The Trap Enclosure

In order to obtain the ultra-high vacuum necessary for long containment times, the trap is mounted in its own vacuum enclosure and cryopumped to 4.2 K. The trap enclosure is constructed of OFHC copper, and indium is used to make the vacuum seal. This system is typically evacuated to around 5 x $10^{-7}$ torr with a turbo-molecular and/or ion pump and lightly baked to 130°$C$ to remove moisture and other adsorbed gases from the electrode and degrader surfaces. The active pump is removed by pinching off an annealed 0.375" OD copper tube [91].

Electrical leads are passed into the trap enclosure, using 24 single conductor feedthroughs [57]. The non-magnetic feedthroughs consist of a 70% Cu-30% Ni base and cap, and have a copper center wire. We soldered these in the copper pinbase at 805°$C$ using Cu-Ag eutectic solder in a hydrogen atmosphere. (The center wire to pinbase capacitance is $\approx$ 8 pF.) There are also six smaller access ports into the enclosure, one on the top center, and 5 on the bottom flange. Two ports are used for additional electric feedthrough access, one for pumpout access, and one has a glass to metal seal to allow 164 GHz microwaves into the vacuum enclosure. The center port on the bottom is connected to a copper flange and tube. The tube is covered with a 10 $\mu$m thick titanium window sandwiched between two titanium rings and electron beam welded together. This thin window is the entrance for the antiproton beam received from LEAR at CERN.

The harmonic trap and the extension electrodes described earlier in this chapter are mounted from the top pinbase using three copper beryllium rods (Fig. 3.4). The trap is kept under slight compression using tungsten springs to accomodate the small length change that occurs when the system is cooled from 300 K to 4 K. The trap support mechanism is referenced to the inner vacuum enclosure walls to

insure vertical alignment.

The top pinbase is designed so that the vacuum enclosure can be removed leaving the entire trap and amplifiers in the electronics region in place or, if so desired, the trap enclosure can be unwired and the sealed vacuum enclosure removed from the rest of the dewar system.

### Floating Thermal Radiation Shield

The entire dewar, electronics region, and trap enclosure are enclosed with an aluminum thermal radiation shield. This shield, which has only 1.5 mm clearance over the dewar system and 4.8 mm to the magnet bore is an essential component for minimizing the radiation heat load from the 77 K magnet bore. Currently the shield is prevented from shorting to the trap enclosure by using nylon screws as spacers. A longer pathlength support system should be introduced to reduce the conduction heat load through this path, although the existing thermal gradient is relatively small.

The tube is wrapped in 2 layers of aluminized mylar to reduce the surface emissivity and is heat sunk to the helium fill and recovery tube in the G-10 thermal isolation region to effectively shunt heat radiated from the 77 K bore into the colder helium gas leaving the center dewar, keeping this shield at temperatures well below 20 K. The shield also protects the delicate wiring when the experiment is inserted in the solenoid.

### Wiring Harness

The apparatus requires about 32 dc leads, 7 RF Transmission lines, 2 high voltage lines, and a 10 GHz microwave pathway. The wiring must not be magnetic, must not conduct much heat to the helium Dewar, and must not take much space. The low voltage dc lines consist of 0.003" diameter constantan wire insulated with a thin coating of teflon [76]. Radiofrequency drives are applied via twisted pairs of these constantan wires. The 50 $\Omega$ detection lines are 0.06" OD coaxial cable with inner and outer conductors made of stainless steel [71]. The high voltage lines are also thin stainless steel coaxial cables interfaced to SHV connectors that have

been modified so that air can be pumped out of their interior regions. Microwaves at 164 GHz are necessary to carry out precision measurements with electrons. Because only small power levels are needed we transmit 10 GHz microwaves to the trap enclosure by using small copper coaxial cable in series with a short piece of stainless steel coaxial cable for thermal isolation, then multiply up to 164 GHz in a diode located near the trap.

Two complete cryogenic and trap systems were constructed to allow rapid replacement if a component failed while antiprotons were available. the possibility also existed to make radical changes or repairs on one system, while taking data with the other. Having two completely independent systems also provided a good opportunity for understanding the level of several important systematics, such as the effect of different trap alignment and imperfections, and the slightly different magnetic field within each system.

### 3.2.2 Performance

Three major heat transfer mechanisms contribute to the heat load on the 4 K liquid helium reservoir. Convection and conduction processes through gas are eliminated by evacuation of the magnet bore to a pressure better the $10^{-5}$ torr. Conduction through the thermal isolation region is minimized by material selection and by maximizing path lengths. A forced thermal shunt to the 77 K magnet bore also allows for a longer pathlength between 77 K and 4 K to the liquid helium Dewar. Absorbed radiation is reduced by low emissivity aluminized mylar surfaces and with the use of the floating radiation shield which takes advantage of the substantial heat capacity (i.e. cooling capacity) of helium gas between 4K and 300 K. The addition of this floating radiation shield properly anchored to the helium fill/recovery line more than tripled the Dewar hold time.

The assembled and tested system described in the previous section is lowered into the magnet bore slowly to allow eddy currents time to dissipate and prevent excessive stress on the magnet coils. The experiment can be installed into the magnet when the magnet bore is at 300 K or 77 K. To prevent moisture conden-

sation when the magnet bore is cold, we flow $N_2$ gas through it whenever it is open.

After the experiment is lowered into position, the magnet bore is pumped to better than $5\times10^{-3}$ torr using a liquid nitrogen cooled sorption pump. This pump provides a smooth and gradual method of rough pumping against the delicate 10 $\mu$m thick titanium windows on the trap enclosure and on the incoming beamline system. The liquid helium Dewar system is precooled with liquid nitrogen, and the temperature of the trap enclosure monitored with a carbon glass resistor. The system reaches thermal equilibrium at 77 K after approximately 12 hours, limited predominantly due to the long time constant to remove the heat from the floating thermal radiation shield. This precool period has been forced to as short as 1.5 hours, but the helium boiloff is then extremely high for the first day requiring at least 2 more refills. After an optimum 12 hour wait or longer, we blow out the remaining liquid nitrogen and fill with liquid helium. The initial cooldown and fill of the 3.7 liter capacity takes approximately 9 liters (including transfer line cooldown losses), and subsequent fills take just under 5 liters. The trap enclosure is at 4.2 K by the time the helium has collected, demonstrating the effectiveness of our gold plated compression joints (no grease is used). Even though the vacuum is sufficient so that the trap can be immediately loaded, the tuned RF circuits have a cooling time constant of a couple hours as observed in the drift of their resonant frequency.

The hold time of the 3.7 liter Dewar in a completely wired state, but with the Field Effect Transistors (FET) off, is 6 days. This corresponds to a boiloff rate of less than 26 ml/hr or a total heat load to the liquid helium reservoir of 18 mW. With all three detection amplifier FET's on continuously, the heat load increases by 50% ($\approx$ 3 mW per amplifier) and the holdtime is reduced to about 4 days.

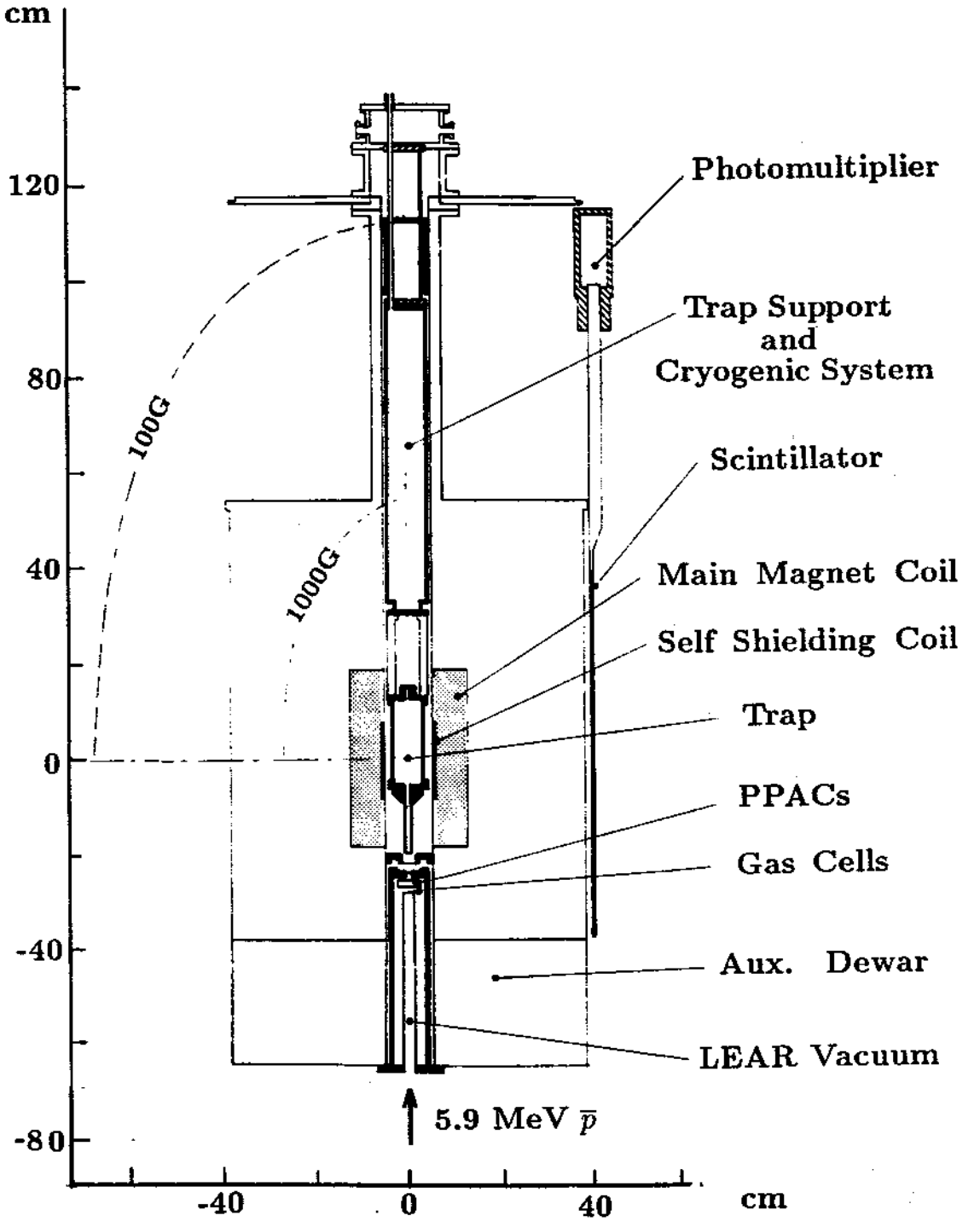


Figure 3.7: The Nalorac superconducting magnet with the antiproton trap and cryogenic system inserted into the bore and interfaced to the LEAR beamline.The magnet has a 100 mm diameter bore that can be cooled to 77 Kelvin.

## 3.3 Shielded Superconducting Magnet

### 3.3.1 Specifications and Field Shimming

The properties of the magnetic field in the trapping region are of crucial importance to the success of the mass comparison technique. Since we observe the modified cyclotron frequency of confined particles, the ultimate precision and accuracy of the measurement directly depends upon the magnetic field homogeneity and time stability over the trapping volume.

Because of the stringent field homogeneity and stability requirements for the highest precision mass comparisons, we acquired a state-of-the-art superconducting solenoid from the Nalorac Cryogenics Corporation [75]. The maximum field strength is 5.9 T and the bore diameter is 100 mm. With such a field strength the antiproton cyclotron frequency is in the FM radio band at about 89 Mhz, requiring a measurement of the cyclotron frequency to better than 0.1 Hz for $10^{-9}$ resolution.

For ease of access to the field center, the vertical magnet has a through bore so that the accelerator may be interfaced to the bottom, and the trapping apparatus inserted from the top (Figs. 3.6, 3.7, and 3.10). The bore of the solenoid is heat sunk to its own liquid nitrogen cryostat and can be operated at room temperature or cooled to 77 K to provide the necessary thermal isolation to maintain the particle trap at liquid helium temperatures. The bore is constructed of an OFHC copper tube to minimize thermal gradients along its length, and is thermally isolated from its external flanges by 15 cm long segments of 100 mm ID G-10 tube.

The main magnet solenoid resides in its own ultra low loss liquid helium cryostat (hold time $\geq$ 3 months), is constructed using single filament niobium titanium wire wound onto an aluminum spool. Differential currents in the main solenoid can be used to create parabolic field contours along the symmetry axis, but for the purpose of the mass comparison, we adjust coil currents to obtain maximum field uniformity along the z axis. Several additional superconducting shim coils allow for field compensation. Axial field correction is provided from zero through third order, and radial correction is provided from zero through second order.

There are also three shims which operate at room temperature allowing for small adjustments to be made at any time. They include shims for slightly changing the uniform field $\Delta B_0$ and the first and second order axial gradients $\Delta B_1(z)$ and $\Delta B_2(z^2)$. The room temperature shim range is measured to be

| Shim | Full Range | Fractional Shift |
|---|---|---|
| $B_0$ | $\pm$ 1.3 G | $\pm$ 22 $\times$ $10^{-6}$ |
| $B_1$ | $\pm$ 1.5 G/cm | $\pm$ 25 $\times$ $10^{-6}$ |
| $B_2$ | $\pm$ 0.2 G/cm$^2$ | $\pm$ 3 $\times$ $10^{-6}$ |

These shims are very useful for cyclotron resonance identification, for tuning out the residual bottle field, and for performing systematic checks.

The decay of the persistent field is specified to be less than 1 part in $10^{-9}$ per hour.

### Pulsed NMR Measurements

To check the magnet specifications and for initial shimming purposes we have constructed a simple pulsed Nuclear Magnetic Resonance (NMR) system. The advantage of such a system is that we are able to shim out field gradients over a much larger volume than is feasible using only confined particles in our Penning trap. The NMR sample is a 1 cm diameter sphere of high purity acetone and we measure the proton NMR precession frequency ($\approx$250 Mhz) at the field center where the Penning trap is to reside. For these measurements, the magnet bore is open to the atmosphere and at room temperature.

The protons in the NMR sample are driven near their natural precession frequency with a strong transverse magnetic field. After a strong drive pulse, the protons precess freely about the magnetic field axis, inducing a signal which is detected by the same coil used to drive them. The precession signal decays over time as the proton nuclear moments This Free Induction Decay(FID), is shown in Fig. 3.8 along with the Fourier transform. The linewidth of this transform is

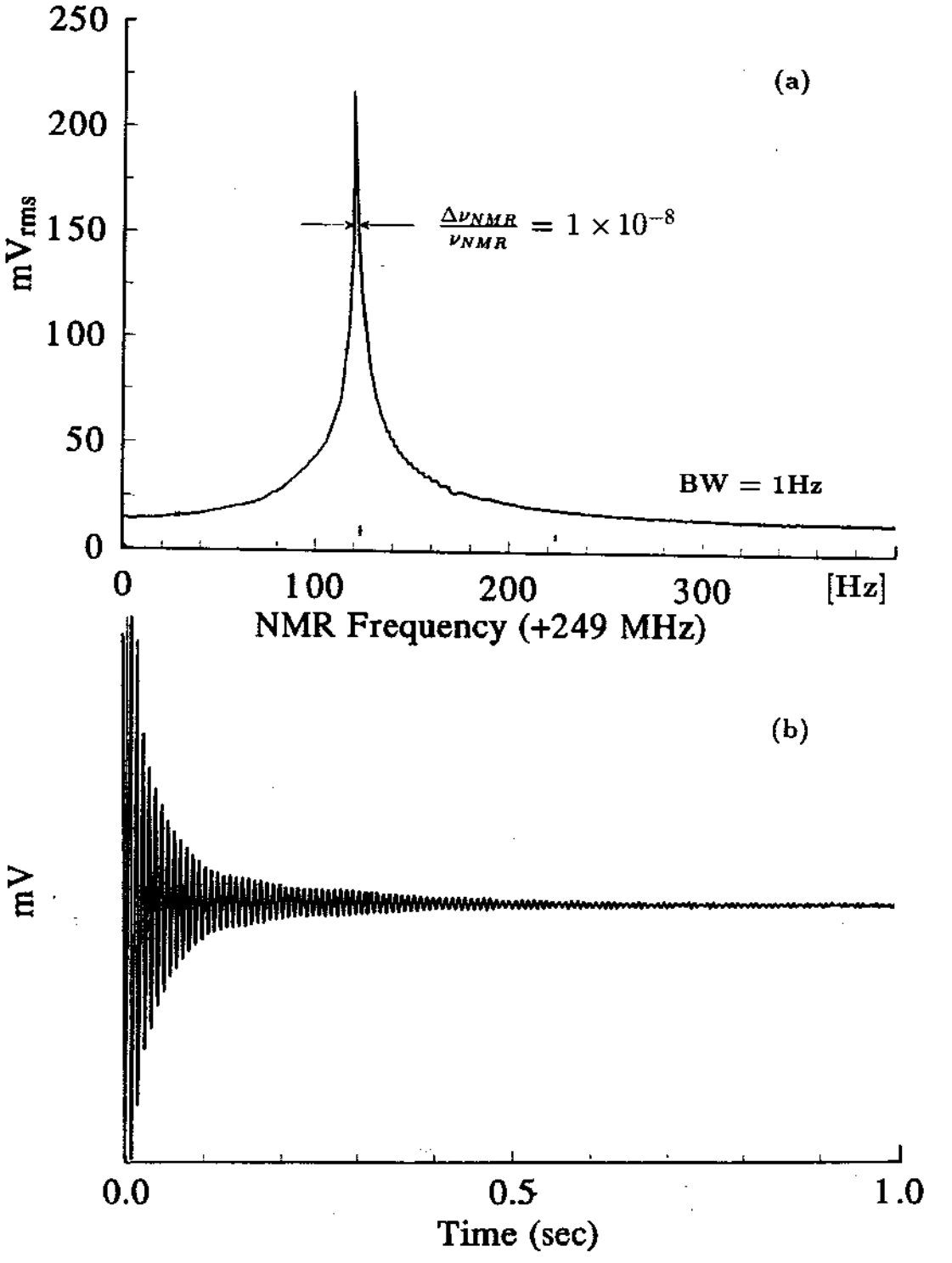


Figure 3.8: (a) Proton NMR signal mixed down from 249 MHz. (a) Fourier transform of the proton precession from a 1cm diameter spherical sample of acetone. The linewidth represents a field homogeneity of $\Delta B/B=10^{-8}$ over the sample volume. (b) Free Induction Decay of the precessing proton spins.

related to magnetic gradients present over the sample volume. By minimizing the Fourier transform linewidth and maximizing the amplitude while we adjust the superconducting shims, we tune out the large magnetic gradients maximizing the homogeneity over the 0.5 $cm^3$ acetone sample.

The gradient fields imposed on the magnet system are quite large in the experimental area, since the experiment is surrounded by very large concrete block walls required for radiation shielding from the nearby accelerator beamlines (see Fig. 3.10). Some of the large concrete blocks, with steel reinforcing inside, are as close as 1 meter from the magnet center. Directly below the superconducting solenoid are large bending magnets necessary to direct upwards the 5.9 MeV antiprotons from LEAR. Fortunately these strong magnetic sources are fixed in space so that most of the gradients imposed by their proximity can be permanently shimmed out of the trapping region by fine adjustment of the magnet currents.

The field can be shimmed using the superconducting shims to 1 part in $10^8$ over the 1 cm diameter sample. The FID of the NMR sample is shown in Fig. 3.8. Unfortunately, by removing and reinserting the NMR probe into the magnet, the resonance can broaden up to 5 parts in $10^7$. This suggests that the fine shimming is related to the NMR probe itself (constructed of aluminum, copper, G-10 and quartz) resulting from its own para- and diamagnetism. For effective shimming and homogeneity measurements at the most precise levels, and to take into account the residual bottle field from the trap electrodes themselves, higher precision measurements of the trapping field homogeneity must be made directly in the actual trap apparatus.

### 3.3.2 Self Shielding System

To compare the masses of the proton and antiproton to a precision of $10^{-9}$ in a 5.9 Tesla magnet requires that the time stability be better than 6 nT (60 $\mu G$) over one hour (a typical time necessary to prepare and compare the cyclotron frequencies of two species of ions). Fluctuations in the earth's magnetic field can vary more than ten times this amount. In many laboratories other sources of magnetic fluctuations, such as elevators and subway lines, have been a common

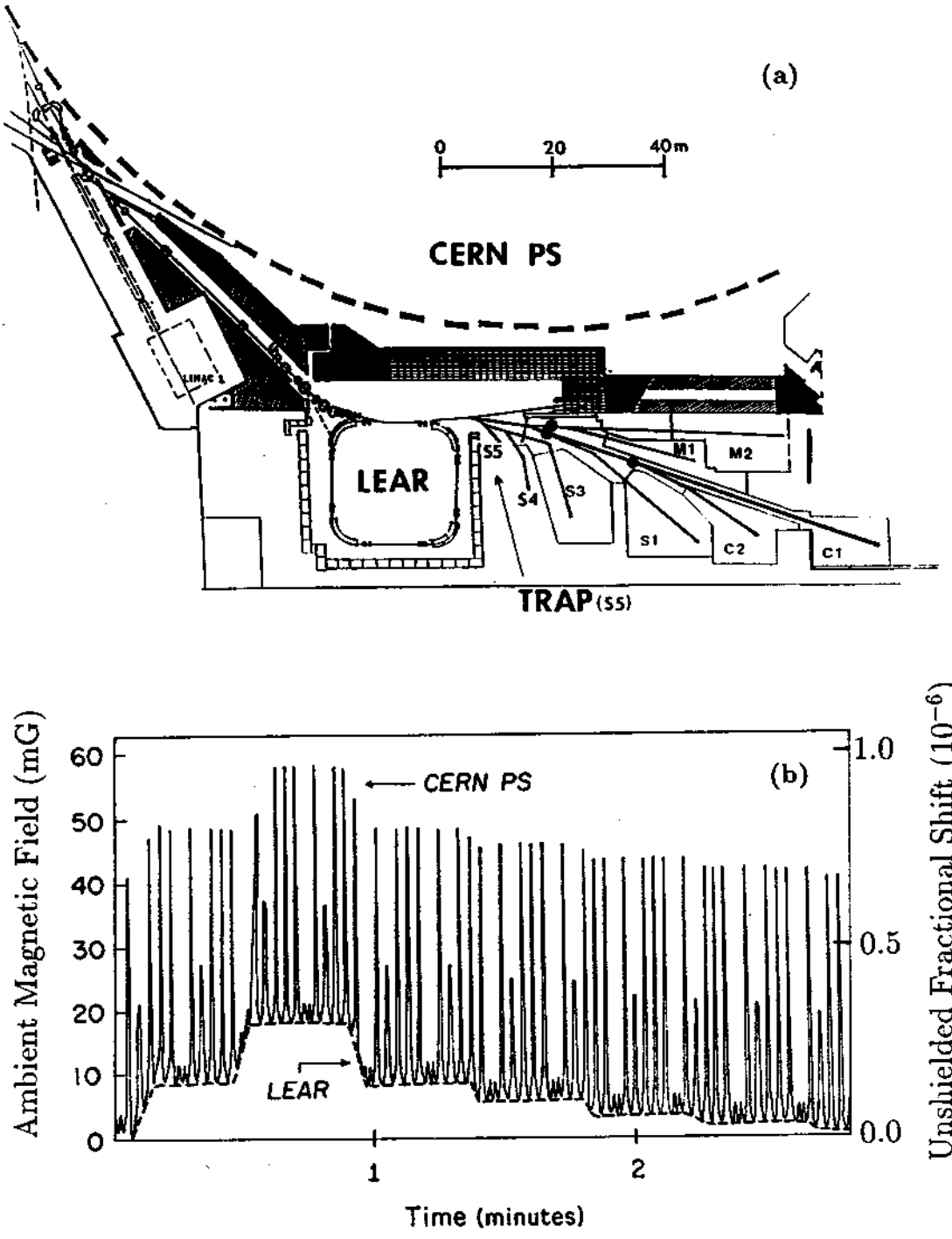


Figure 3.9: (a) LEAR and associated experimental areas with the CERN PS shown nearby. The trapping apparatus is located in zone S5. (b) Magnetic field fluctuations in zone S5 resulting from the PS and LEAR cycling their respective magnets. (The typical LEAR cycle takes about 15 minutes and is of opposite polarity shown here).

hindrance to the accuracy achievable in high precision measurements. Our need for antiprotons, which can only be obtained at high energy accelerator facilities, presents us with the difficult challenge of doing high precision mass spectroscopy in an environment where magnetic field perturbations can be much larger than normal.

Our experiment is located only 8 meters from the Low Energy Antiproton Ring, and approximately 19 meters from the Proton-Synchrotron of CERN (Fig. 3.9). In addition, two large 5.9 Mev bending magnets are 1 meter below our superconducting solenoid (Fig. 3.10), and two very large steel overhead cranes can move to within 2 meters of the magnet. A detailed quantification of the field in the experimental hall is given in Chapter 10, but it suffices here to note that the largest controllable fluctuations (e.g. from our bending magnet), are on the order of 20 $\mu$T (0.2 G) and the largest uncontrollable on the order of 4 $\mu$T (0.04 G). If there existed no field compensation at the center of the trap, the uncontrollable fluctuations would correspond to fractional changes in the trapping field of up to 7 parts in $10^7$. While careful selection of measurement times avoids some of the largest perturbations, screening of the ambient field fluctuations is of prime importance towards success of the experiment. Passive shielding constructed of high permeability materials such as $\mu$-metal is not feasible since they would saturate in the high field unless located farther from the superconducting solenoid than available space will allow. Type I superconductors such as lead or niobium cannot be used since the large magnetic field (several Tesla) is above their critical field. Active feedback to e.g. a Helmholtz coil could possibly be incorporated using a second sensor probe near the trap center at 4 K (e.g. a second particle trap or a $^3$He NMR probe).

The solenoid provides partial self screening to external fluctuations, measured to be about a factor of -4.27(7) [46]. At best this reduces uncontrollable fluctuations to about $2\times10^{-7}$, still far from our ultimate goal of comparing the antiproton and proton masses beyond the $10^{-9}$ level. To obtain further screening, we had our Nalorac magnet fitted with an additional superconducting coil with dimensions based on a computation by Gabrielse and Tan [42]. The idea takes advantage

of the flux preserving properties of a superconducting coil. With the proper coil geometry, the induced current in the shielding coil resulting from a change in the ambient field generates a magnetic field at the coil center (the trap location) which is equal in magnitude but opposite in direction to the ambient fluctuation. Thus the effective magnetic field at the trap center where the trapped particles reside remains essentially constant.

In the relatively quiet laboratory at Harvard University, we measured the effectiveness of the additional shielding coil using pulsed NMR and by applying a nearly uniform magnetic field with two square coils 2.81 meters on a side and separated by 1.53 meters. The shielding was measured to be [46]

$$S = \frac{\Delta B_{outside}}{\Delta B_{inside}} = -156(6). \tag{3.19}$$

This is a significant improvement which greatly aids our ability to perform the antiproton mass comparison in the experimental hall at CERN. In addition to the shielding, the same NMR linewidth is observed with the shielding coil as without it, indicating that the spatial homogeneity is not compromised over the 1 cm diameter spherical volume of the NMR sample.

The shielding system is most effective for shielding spatially uniform fluctuations and linear gradients in the ambient field [42]. Since the experiment is located in an accelerator environment, the field fluctuations from nearby sources have a component which is not spatially uniform. Fluctuations are further distorted by the large amounts of ferromagnetic steel in the concrete shielding, resulting in a shielding factor which varies as a function of the source (see Chapter 10).

## 3.4 RF Shielding and Grounding

For mass spectroscopy with RF techniques, isolation from the ambient radio frequency environment is important. At CERN, the RF environment is especially troublesome because of the current switching and RF generation used for accelerating particles. The detected signals are small and, in addition, the cyclotron frequency of the antiproton is in the FM radio band and the antiproton axial fre-

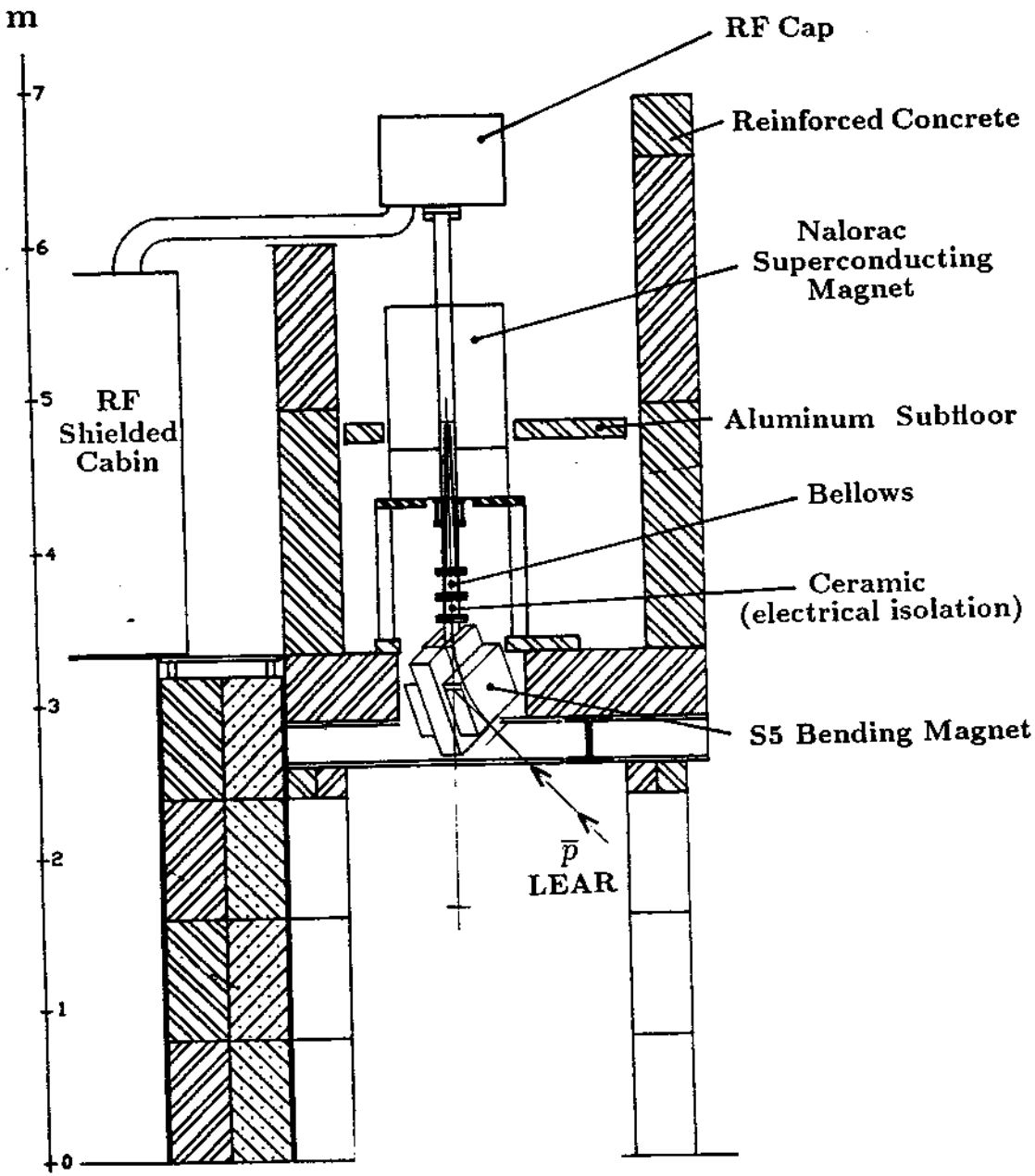


Figure 3.10: An overall view of the experimental zone showing the Nalorac magnet and the RF shielded region.

quency is near the AM radio band. If such signals leak into the trap, they may heat the particle motions.

There are many space constraints in the area of our experiment and placing the whole experiment in an RF enclosure was not possible. Instead, we have a smaller RF shielded cabin for the drive and detection electronics as shown in Fig. 3.10. The RF cabin is connected to the magnet vacuum enclosure using a large diameter corrugated aluminum tube containing all the electrical leads (mostly double shielded coaxial cables) between the electronic cabin and the trap apparatus located in the magnet bore. The cabin, tube, and magnet vacuum enclosure form a grounded RF shield. Part of the grounded 'shield' is a 30" diameter aluminum plate bolted on the top of the magnet. Amplifiers and other electronics which need to be physically close to the trap are bolted here. The region over the magnet is covered with an aluminum cap to complete the RF shield, and the magnet is electrically uncoupled from the LEAR complex by a ceramic connection to the beamline just below the superconducting solenoid.

Unfortunately, not all of the leads to the experiment access through the RF cap. Several leads are required for antiproton beam diagnostics at the bottom of the magnet. In addition, the cryogenic level sensor lines and the room temperature magnet shim leads enter the magnet from points outside of the RF cage formed by the cabin, tube, cap, and magnet bore. These external lines can be troublesome for allowing unwanted RF into the system either directly or perhaps by closing a ground loop. Generally, these are disconnected during the most sensitive measurements.